Biodistribution, PET, and Radiation Dosimetry Estimates of HSV-tk Gene Expression Imaging Agent 1-(2′-Deoxy-2′-^{18}F-Fluoro-β-D-Arabinofuranosyl)-5-Iodouracil in Normal Dogs

Sridhar Nimmagadda[1,2], Thomas J. Mangner[1,3], Kirk A. Douglas[1,2], Otto Muzik[1,4], and Anthony F. Shields[1,2]

[1]Karmanos Cancer Institute, Wayne State University, Detroit, Michigan; [2]Department of Medicine, Wayne State University, Detroit, Michigan; [3]Department of Radiology, Wayne State University, Detroit, Michigan; and [4]Department of Pediatrics, Wayne State University, Detroit, Michigan

FIAU is of interest as a potential reporter probe to monitor herpes simplex virus thymidine kinase (HSV-tk) gene expression and bacterial infections. This study investigates the biodistribution, metabolism, and DNA uptake of 1-(2′-deoxy-2′-^{18}F-fluoro-β-D-arabinofuranosyl)-5-iodouracil (^{18}F-FIAU) in normal dogs. **Methods:** Four normal dogs were intravenously administered ^{18}F-FIAU. A dynamic PET scan was performed for 60 min over the upper abdomen; this was followed by a whole-body scan for a total of 150 min on 3 dogs. The fourth dog was not scanned and was euthanized at 60 min. Blood and urine samples were collected at stipulated time intervals and analyzed by high-performance liquid chromatography to evaluate tracer clearance and metabolism. Tissue samples collected from various organs were analyzed to evaluate tracer uptake and DNA incorporation. Dynamic accumulation of the tracer in different organs was derived from reconstructed PET images. Nondecay-corrected time–activity curves were used for residence time calculation and absorbed dose estimation. **Results:** At 60 min after injection, unmetabolized FIAU radioactivity in blood and urine samples was greater than 78% and 63%, respectively, demonstrating resistance to metabolism. The tissue-to-muscle ratio derived from image and tissue analysis showed a slightly higher uptake in proliferating organs (mean tissue-to-muscle values: small intestine, 1.97; marrow, 1.70) compared with nonproliferative organs (heart, 1.07; lung, 1.06). A high concentration of activity was seen in the bile (mean, 23.02), demonstrating hepatobiliary excretion of the tracer. Extraction analysis of tissue samples showed that >62% of the activity in the small intestine, 74% in marrow, and <21% in heart, liver, and muscle was incorporated into DNA. **Conclusion:** These results demonstrate that FIAU is resistant to metabolism and moderately incorporates into DNA in proliferating tissues. These results suggest that incorporation into the DNA of normal tissues may need to be considered when FIAU is used to track reporter gene activity. Studies in humans are needed to determine whether imaging properties differ in patients and are altered as a result of metabolism changes affected by gene therapies.

Key Words: ^{18}F; FIAU; metabolism; gene expression imaging; herpes simplex virus thymidine kinase

J Nucl Med 2007; 48:655–660
DOI: 10.2967/jnumed.106.036830

Many pyrimidine and acycloguanosine analogs have been investigated as reporter probes for herpes simplex virus thymidine kinase (HSV-TK). An overview of the analogs has been briefly reviewed in the literature (*1*). Of all analogs tested to date, fialuridine, 1-(2′-deoxy-2′-fluoro-β-D-arabinofuranosyl)-5-iodouracil (FIAU), and 1-(2′-deoxy-2′-fluoro-β-D-arabinofuranosyl)-5-ethyluracil (FEAU) seem to be promising tracers for wt-HSV-tk and 9-(4-fluoro-3-hydroxymethylbutyl)guanine (FHBG) for HSV-sr39tk (*2*) gene expression imaging. FEAU is perhaps the most sensitive and specific tracer for both wild-type and mutant 39tk gene expression imaging (*1*). However, FEAU requires toxicity information before it can be used in a clinical setting. To date, studies indicate that FIAU has the greatest potential use as a clinical imaging agent to monitor gene expression.

Use of 5-halogen–substituted nucleoside analogs as proliferation and gene expression imaging agents has been well investigated. Deiodination of 5-halogen analogs may be a problem for ^{18}F-labeled compounds because of the possibility of active metabolite contribution to the images. In the case of radioiodinated FIAU, the metabolite is a nonradioactive 1-(2′-deoxy-2′-fluoro-β-D-arabinofuranosyl)uracil (FAU); however, ^{18}F-FIAU deiodination results in ^{18}F-FAU. ^{18}F-FAU may be converted to 1-(2′-deoxy-2′-fluoro-1-β-D-arabinofuranosyl)-5-methyluracil (^{18}F-FMAU). Although ^{18}F-FAU incorporation into DNA is limited and its substrate characteristics to viral and bacterial thymidine kinases

Received Oct. 7, 2006; revision accepted Dec. 15, 2006.
For correspondence or reprints contact: Anthony F. Shields, MD, PhD, Karmanos Cancer Institute, 4100 John R St., 4 HWCRC, Detroit, MI 48201-2013.
E-mail: shieldsa@karmanos.org

have yet to be established, the role of ^{18}F-FMAU as a proliferation marker has been demonstrated (*3*). The complexity of metabolite formation, their various roles, and possible contribution to images merits a detailed analysis of the metabolic properties of ^{18}F-FIAU.

^{18}F-FIAU is more suitable to monitor HSV-Tk or other viral and bacterial thymidine kinase expression in a clinical setting (*4*) due to its favorable dosimetry characteristics. Jacobs et al. have successfully used ^{124}I-FIAU to monitor the HSV-tk transduction in human gliomas (*5,6*). Considering its clinical potential, this PET study describes the biodistribution, metabolism, and dosimetry characteristics of ^{18}F-FIAU in normal dogs.

MATERIALS AND METHODS

Synthesis of ^{18}F-FIAU

^{18}F-FIAU was synthesized as previously described using 2,4-bis-*O*-(trimethylsilyl)-5-iodouracil as an intermediate precursor (*7*). The total synthesis uncorrected radiochemical yields were 34.5% (n = 4; range, 23.1%–40.2%) with >98% radiochemical purity and 222 GBq/μmol (6 Ci/μmol) specific activity. The total synthesis time was 188 min (range, 142–212 min).

PET Acquisition and Analysis

All experimental procedures using the animals were conducted according to a protocol approved by the Animal Investigation Committee of Wayne State University. Four normal dogs of mixed breeds weighing between 12.8 and 20 kg (mean weight, 17.1 kg) were used for biodistribution and imaging studies. Of these, 3 of the dogs underwent both imaging and biodistribution studies. The fourth dog was not scanned and was euthanized at 60 min after injection. All animals were premedicated with acepromazine (0.1–0.5 mg/kg); anesthesia was induced with pentobarbital (10–25 mg/kg) and maintained with isoflurane (1.5%–3.0%).

Before injection of the tracer, a 15-min transmission scan was obtained to correct for photon attenuation within the body. The tracer ^{18}F-FIAU (mean activity, 303 MBq; range, 241–370 MBq, in 5 mL) was administered as a slow bolus over 1 min using an infusion pump (Harvard Apparatus Inc.). Coinciding with tracer injection, a 60-min dynamic scan (24 frames: 4 × 20 s, 4 × 40 s, 4 × 60 s, 4 × 180 s, 8 × 300 s) was acquired over the upper abdomen; this was followed by a static whole-body scan for a total of 150 min. All images were acquired on an ECAT EXACT HR PET scanner (Siemens Medical Solutions USA, Inc.) in 2-dimensional mode, yielding 47 contiguous slices with a slice thickness of 3.12 mm.

Dynamic and whole-body images were reconstructed and image analysis was performed as described (*8*). Circular regions of interest (approximate radius, 17.6–13.2 mm) were drawn on the lungs, heart, muscle, marrow (8.8 mm), kidneys, liver, and intestine to obtain the concentration of ^{18}F versus time in μCi/mL. The standardized uptake values (SUVs) were calculated by dividing tissue radioactivity concentration (MBq/mL) by the injected radioactivity (MBq) per gram of body weight (assuming 1 mL = 1 g). The decay-corrected time–activity values were averaged over 3 animals.

Blood and Tissue Analysis

All data regarding blood and tissue sample acquisition were obtained as described (*8*). Briefly, blood samples were drawn at 1, 2, 3, 4, 5, 6, 7, 9, 11, 15, 21, 30, 40, 50, 60, 90, 120, and 150 min after injection, and urine samples were collected at 60 and 120 min to measure the metabolite concentration. Total blood and urine activity was measured in a NaI(Tl) well counter cross-calibrated with the PET camera (Cobra II; PerkinElmer Life Sciences Inc.). For metabolite analysis, selective blood samples were processed with 1 M perchloric acid as described earlier (*8*). Supernatants were analyzed by high-performance liquid chromatography (HPLC) using a C-18 column (Hypersil ODS, 250 × 4.6 mm; Thermo Electron Corp.) with 10 mM sodium acetate in 6% acetonitrile as a mobile phase at a flow rate of 1 mL/min.

At the end of the experiment, the animals were sacrificed; samples of heart, kidney, lung, liver, muscle, marrow, node, spleen, stomach, small intestine, and bile were collected (200–300 mg), weighed, and measured in a γ-counter for 1 min before DNA extraction analysis. Samples of liver, muscle, heart, small intestine, and marrow were homogenized (Tissue Tearor; Biospec Products Inc.) and extracted with 1 mL of 1 M perchloric acid. After the extraction, all supernatants and pellets were counted on the γ-counter and the activity values were converted into SUVs. The supernatants from the first extraction were analyzed by HPLC for metabolite analysis.

Identification of Metabolites in ^{18}F-FIAU Blood Samples

To identify the polar metabolite observed in blood, samples from the 60-min time point had 740 kBq of ^{3}H-FAU added as a reference standard. HPLC analysis of the processed blood sample was performed on a C-18 column as described, but with a flow rate of 0.5 mL/min. All fractions were first counted on a cross-calibrated γ-counter to determine the ^{18}F activity. On the following day, HPLC fractions were mixed with 5 mL of Ultima Gold scintillation cocktail (Packard Bioscience), chilled overnight, and counted for 5 min using external standard quench correction to account for ^{3}H activity.

Dosimetry Analysis

Nondecay-corrected time–activity curves for different organs were calculated as described in the PET analysis section. Corresponding tracer concentration at a later time point was obtained from the whole-body image at approximately 2.5 h. From the last data acquisition time point to infinity, tracer activity was presumed to follow the physical decay of ^{18}F. The area under the curve (AUC) for each organ was calculated using the trapezoidal method, and the residence time (min) for each organ was subsequently calculated by dividing the AUC (MBq/mL × min) with the injected dose (MBq) and multiplied with the corresponding organ weight (g). As the bladder concentration was available only from the whole-body image, the bladder residence time was calculated based on a constant bladder concentration from the start of the study until the measured time point.

The radiation-absorbed doses in humans were estimated using the organ residence times calculated from normal dogs using the scheme of a 70-kg man in the OLINDA/EXM version 1.0 program (*9*).

RESULTS

Imaging and Kinetics of ^{18}F-FIAU

Figures 1A and 1B illustrate the projection and sagittal slices of whole-body images obtained between approximately 60 and 150 min after injection of ^{18}F-FIAU. From the images it is clear that ^{18}F-FIAU does not show

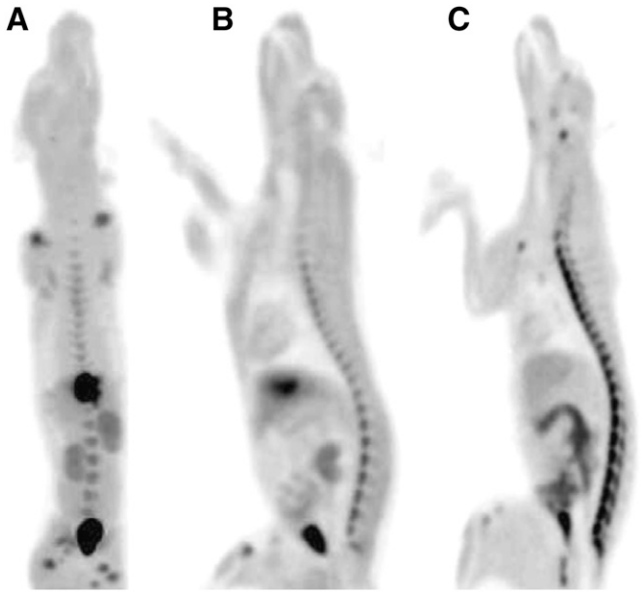

FIGURE 1. Representative projection (A) and sagittal (B) PET images of dog acquired between 70 and 150 min after injection of 274 MBq of ^{18}F-FIAU. Activity above background could be seen in marrow, kidneys, heart, and small intestine. (C) For comparison, sagittal view of a dog injected with proliferation marker 1-(2′-deoxy-2′-fluoro-1-β-D-arabinofuranosyl)-5-bromouracil. Both images were adjusted to same maximum SUV.

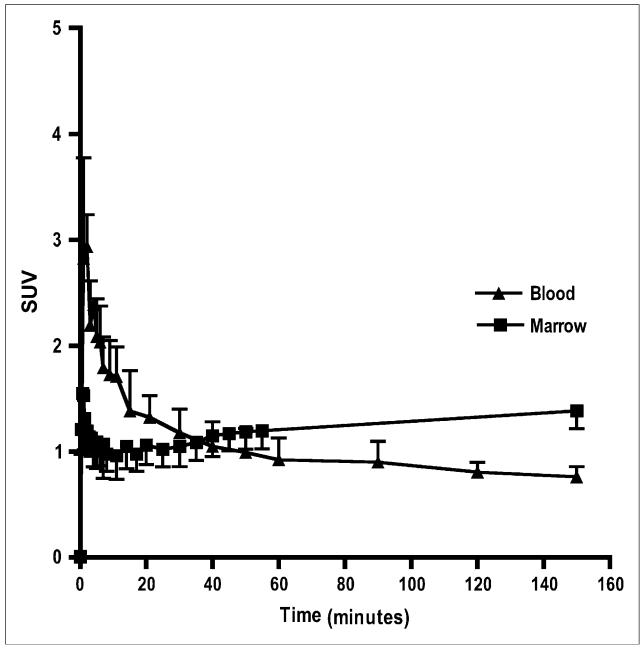

FIGURE 2. Mean blood and marrow time–activity curves of FIAU in normal dogs. Activity is cleared from blood after showing initial peak. Even though marrow shows low uptake before 50 min, slow accumulation of activity could be seen over 150 min.

strikingly specific uptake in any tissue other than gallbladder and bladder, which are excretory organs. Other tissues with marginal activity that could be seen above the background were marrow, small intestine, and kidneys. The heart, though clearly visible, is only seen next to the low activity in the lungs.

The blood activity curve for ^{18}F-FIAU showed an early peak and then a rapid decrease similar to that observed with other thymidine analogs. Most of the activity was cleared by 60 min after injection. Marrow showed a slow uptake of ^{18}F-FIAU over time, reaching a plateau over 150 min (Fig. 2).

Whereas organs such as liver had an initial peak followed by a fast washout of the tracer, kidneys showed rather slow clearance of the tracer. The time–activity curve for the gallbladder showed increased activity after 10 min that is mostly due to the clearance of the tracer from blood. After 15 min of injection, at all subsequent times, the retention of the tracer in the gallbladder was substantially higher than activity levels in all other tissues (Fig. 3).

Biodistribution of ^{18}F-FIAU

Ex vivo activity measurements for various tissues showed the highest activity in the bile and urine. Also, slightly higher uptake was observed in organs with high proliferation rates, such as the small intestine (mean tissue-to-muscle ratio, 1.97; range, 1.50–2.60) and marrow (mean, 1.75; range, 1.56–1.94), when compared with nonproliferative organs, such as heart (mean, 1.07; range, 0.90–1.39), lung (mean, 1.06; range, 0.94–1.19), and liver (mean, 1.48; range, 1.24–1.65). High uptake was seen in the bile (mean, 23.0; range, 10.3–30.2) due to excretion of the tracer (Fig. 4). Extraction analysis showed that 62% (range, 57%–70%) of the activity in small intestine; 74% (range, 58%–90%) in marrow; and <21%, on average, in heart (range, 6%–14%),

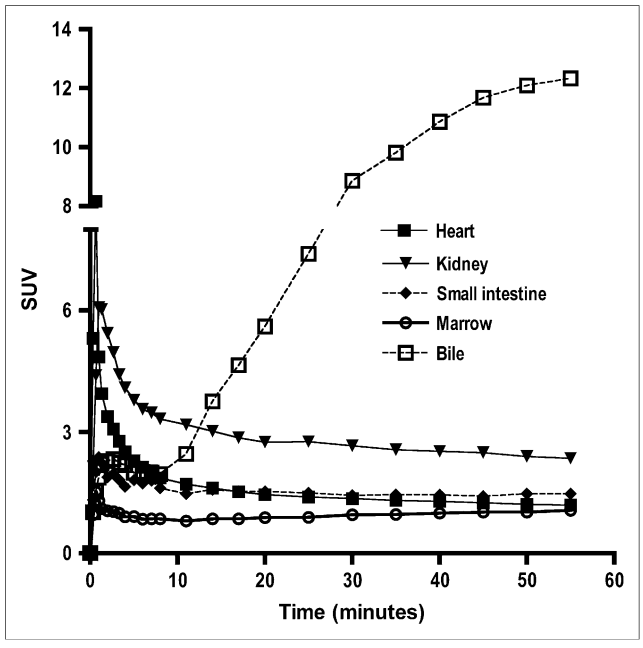

FIGURE 3. Decay-corrected mean time–activity curves in various organs of FIAU-injected normal dogs. Data were acquired up to 60 min after injection. For clarity, SDs are not included.

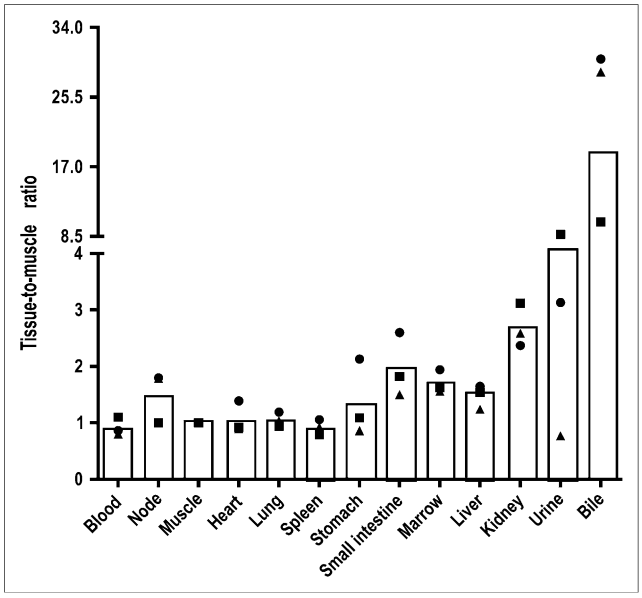

FIGURE 4. Bar graph shows tissue distribution data of normal dogs that received intravenous injection of ^{18}F-FIAU. Uptake is represented as tissue-to-muscle ratio. Ex vivo biodistribution was determined at 150 min after injection. Distribution of data for individual dogs is also shown: ■, dog 1; ▲, dog 2; ●, dog 3.

liver (range, 6%–35%), and muscle (range, 3%–15%) was incorporated into DNA (Fig. 5).

HPLC analysis of blood and urine samples (n = 8; column recovery range, 84%–97%) taken at 60 min found more than 78% (n = 4; range, 61%–90%) and 63% (n = 4; range, 46%–72%) of the radioactivity as unmetabolized ^{18}F-FIAU, respectively. HPLC analysis of the 60-min blood sample, mixed with ^{3}H-FAU as an internal standard, showed that both ^{18}F and ^{3}H activities elute at the same retention time, suggesting the metabolite formed is ^{18}F-FAU (Fig. 6).

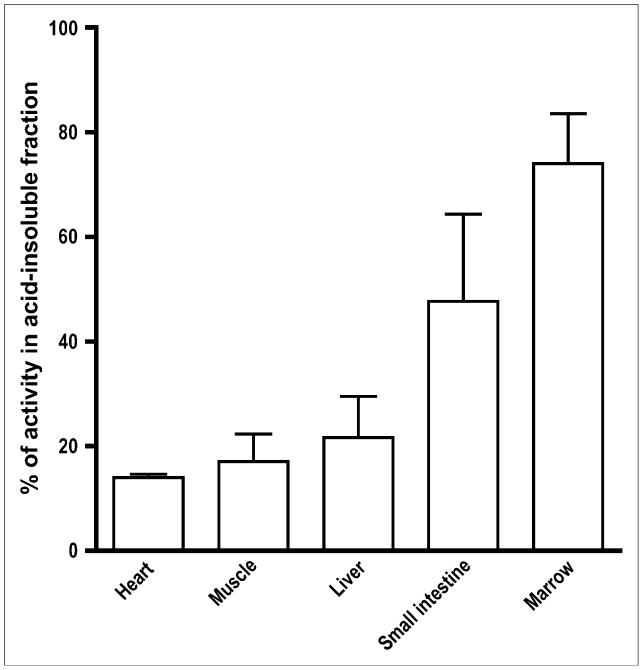

FIGURE 5. Bar graph shows percentage of activity in acid-insoluble fraction from DNA extraction analysis of proliferative and nonproliferative tissue. Graphs show mean ± SD.

Radiation Dosimetry Projections

The radiation dose estimates for the administration of ^{18}F-FIAU to humans are shown in Table 1. The organs with highest radiation burden (μSv/MBq) were gallbladder (90.8), urinary bladder wall (59.6), kidneys (27.2), liver (23.4), and small intestine (21.9), with an effective dose and effective dose equivalent of 14.3 and 21.2 μSv/MBq, respectively.

DISCUSSION

For nearly a decade reporter gene strategies have been used in PET to visualize and monitor various biologic processes, including transcriptional regulation (*10*), lymphocyte migration (*11,12*), and stem cell tracking (*13,14*). The commonly used reporter gene system is the combination of HSV-tk as the PET reporter gene and the pyrimidine analog FIAU as a PET reporter probe (*15*). The HSV-TK and FIAU combination has been well characterized using ^{131}I (half-life [$t_{1/2}$] = 8.01 d), ^{123}I ($t_{1/2}$ = 13.13 h), and ^{124}I ($t_{1/2}$ = 4.2 d) for planar, SPECT, and PET imaging (*15,16*), respectively. Use of these radioiodinated analogs requires large quantities of activity to compensate for deiodination and, subsequently, longer wait times for the clearance of the background activity. Routine clinical use is limited by poor positron yield per decay (27%) and limited availability of ^{124}I. On the other hand, these longer half-life radionuclides are very useful when protracted studies are required, and the commercial availability of ^{124}I (IBA Molecular) may

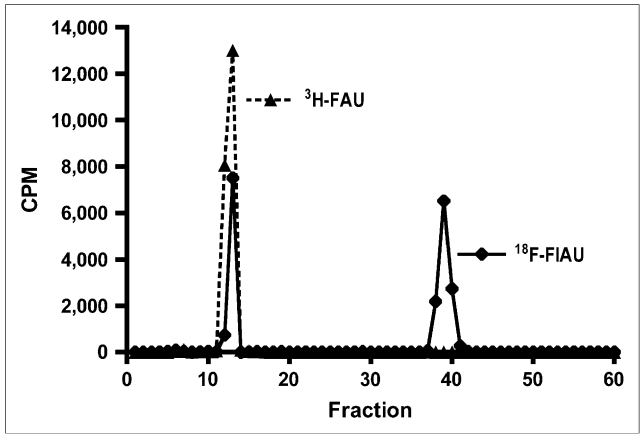

FIGURE 6. Representative reversed-phase HPLC chromatogram of 60-min plasma sample. Standard ^{3}H-FAU was added to blood sample before processing. HPLC fractions were counted on same day for ^{18}F activity and on following day for ^{3}H activity. Retention time for ^{18}F-FIAU metabolite is same as that of FAU. ^{18}F-FIAU peak = 61%.

TABLE 1
Human Organ and Whole-Body Radiation-Absorbed Dose Estimates (Mean ± SD)

Target organ	Mean absorbed dose ± SD	
	μSv/MBq	mrem/mCi
Adrenals	13.53 ± 0.31	50.07 ± 1.10
Brain	8.75 ± 0.21	32.33 ± 0.85
Breasts	8.03 ± 0.07	29.83 ± 0.29
Gallbladder wall	90.87 ± 11.39	336.00 ± 42.32
LLI wall	13.40 ± 0.20	49.73 ± 0.83
Small intestine	21.90 ± 2.50	80.97 ± 9.05
Stomach	12.50 ± 0.30	46.13 ± 0.99
ULI wall	14.43 ± 0.50	53.60 ± 2.09
Heart wall	17.63 ± 0.64	65.30 ± 2.36
Kidneys	27.27 ± 1.34	101.10 ± 5.18
Liver	23.43 ± 3.81	86.80 ± 13.88
Lungs	9.54 ± 1.37	35.27 ± 5.09
Muscle	10.93 ± 0.25	40.60 ± 0.72
Ovaries	14.13 ± 0.58	52.30 ± 2.08
Pancreas	14.30 ± 0.30	52.93 ± 1.00
Red marrow	10.17 ± 0.06	37.77 ± 0.32
Osteogenic cells	14.40 ± 0.26	53.27 ± 0.83
Skin	7.41 ± 0.10	27.33 ± 0.42
Spleen	11.27 ± 0.12	41.53 ± 0.61
Testes	10.20 ± 0.26	37.67 ± 1.07
Thymus	10.04 ± 0.10	37.20 ± 0.20
Thyroid	10.57 ± 0.35	39.17 ± 1.20
Urinary bladder wall	59.63 ± 7.52	220.67 ± 27.93
Uterus	16.03 ± 0.67	59.40 ± 2.55
Total body	12.07 ± 0.06	44.73 ± 0.25
EDE	21.23 ± 0.96	78.73 ± 3.58
ED	14.33 ± 0.25	53.13 ± 1.07

LLI = lower large intestine; ULI = upper large intestine; EDE = effective dose equivalent; ED = effective dose.

Radiation-absorbed doses were extrapolated from ^{18}F-FIAU-injected dog biodistribution data using the OLINDA/EXM version 1.0 computer program.

intensify the use of ^{124}I-FIAU for routine clinical use. In this study we have used ^{18}F-FIAU. Labeling with ^{18}F is superior due its wider availability, better dosimetry characteristics, and favorable yield for decay to positrons (96.9%).

Initial studies of ^{18}F-FIAU in normal dogs have shown even distribution in most organs aside from excretion in the gallbladder and activity in proliferative tissues. For example, uptake above the background was seen in the marrow and small intestine that are clearly visible in the whole-body images acquired between 60 and 150 min (Fig. 1). The time–activity curves acquired over 60 min show a gradual accumulation of activity in the marrow even though total activity is low in comparison with other tissue (Fig. 2). Despite these low levels, activity accumulation could be seen until the end of the study, 150 min. In addition, the acid extraction analysis found greater than 62% and 74% of activity in the small intestine and marrow in the acid-insoluble fraction. This suggests that most of the activity accumulated in the marrow is incorporated into DNA, despite the relatively low affinity of mammalian TK for FIAU (*17*). The limited ^{18}F-FIAU incorporation into DNA is likely to be the source of activity seen in the marrow in the whole-body images. In a recent report, Buursama et al. note that, in spite of high affinity for HSV-TK, FIAU also showed appreciable phosphorylation by mammalian TK when incubated with wild-type and HSV-tk transfected C6 cells with a C6tk-to-C6 ratio of only 10.3 (*18*). Other gene expression agents, FEAU and FHBG, show C6tk-to-C6 ratios of 84.5 and 40.8, respectively. In addition, DNA incorporation of FIAU has been previously demonstrated in vitro in human MOLT-4 cells and in vivo in various tissues of different animals, such as mice, rats, and dogs (*19,20*).

The activity seen in the kidneys, gallbladder, and bladder suggests that ^{18}F-FIAU elimination is due to hepatobiliary and renal clearance. HPLC analyses of blood and urine samples show ^{18}F-FIAU to be reasonably stable. At 60 min after injection, more than 78% and 63% of activity is in the native form. The metabolite formed, ^{18}F-FAU, as determined by using ^{3}H-FAU as a standard, could cause complications if ^{18}F-FAU shows considerable affinity for mammalian, viral, or bacterial TK of interest. The formation of another ^{18}F metabolite of qualitative and quantitative significance, similar to ^{11}C-thymidine, might complicate the use of ^{18}F-FIAU in a clinical setting. Previous studies with ^{18}F-FAU have found the tracer to be uniformly distributed throughout the body, with a low uptake in the marrow (*21*). Similar contrast was also seen in human subjects (*3*). This literature further supports the finding that the uptake we have seen in the marrow of normal dogs is primarily due to ^{18}F-FIAU and not due to ^{18}F-FAU. Once ^{18}F-FAU is formed, it is very stable and shows fast clearance. Studies have demonstrated that >95% of ^{18}F-FAU injected in dogs and humans is in its native form at 60 min after injection (*21*). The in vivo stability of FAU and the absence of radioactive peaks corresponding to FMAU and fluoride both in blood and tissue extracts from ^{18}F-FIAU-injected dogs also rule out the possibility of fluoride and FMAU accumulation in the marrow.

Although both in vitro and in vivo studies indicate that FAU affinity for the mammalian TK is quite low (*21*), studies need to determine the sensitivity of FAU to HSV-TK and its contribution to the images while monitoring HSV-tk gene expression.

In addition, ^{18}F-FIAU is deiodinated gradually over time even though the rate of deiodination might vary between different species. This has been observed in studies in which ^{18}F-FIAU is metabolized faster in mice (50%; S. Nimmagadda, unpublished data, 2005) than in normal dogs (27%) at 60 min after injection. HPLC analysis of extracts from blood and tissue samples did not indicate any defluorination of the tracer within the study period. In contrast, in this study with ^{18}F-FIAU in normal dogs, ^{131}I-FIAU seems to be quite stable in human plasma and whole blood, with >98% of activity in the native form after

24 h (*22*). These variations in deiodination indicate the altered metabolism of the tracer in various species.

Literature reports indicate that FIAU has several potential applications beyond gene expression imaging. Recent developments illustrate that radioiodinated FIAU could be used to image various biologic processes such as bacterial infection (*4*), lytic induction of various viral kinases such as Epstein–Barr virus (EBV) and Kaposi's sarcoma-associated herpesvirus (KSHV) (*23*), and treatment of EBV- and KSHV-associated tumors (*24*). While the merit of other agents, such as FEAU, to image these biologic processes and the associated therapeutic approaches is yet to be demonstrated, radioiodinated or ^{18}F-FIAU might play an important role in clinical decision making.

In the present study, projected absorbed doses in humans indicate only modest exposure, with an effective dose of 14.33 μSv/MBq. For a clinical dose of 370 MBq, this would result in approximately 5.2–5.3 mSv, which would allow for multiple PET studies per year. Under the conservative estimation, the organ with the highest radiation burden is gallbladder wall, followed by urinary bladder wall, kidneys, liver, and small intestine.

CONCLUSION

Studies in normal dogs demonstrated that ^{18}F-FIAU is resistant to metabolism and shows low incorporation into DNA in proliferating tissues. These results support the use of ^{18}F-FIAU to image the distribution of HSV-tk reporter gene in studies of gene therapy. However, incorporation into DNA of normal tissues may need to be considered.

ACKNOWLEDGMENTS

The authors thank Dr. Haihao Sun and Jawana Lawhorn-Crews for their assistance during necropsy; Dr. Elizabeth Dawe, Janet Scaffolding, and Karen Forman for veterinary assistance; and Theresa Jones for imaging support. This work is partially supported by grants CA83131 and CA38566 from the National Cancer Institute.

REFERENCES

1. Kang KW, Min JJ, Chen X, Gambhir SS. Comparison of [^{14}C]FMAU, [^{3}H]FEAU, [^{14}C]FIAU, and [^{3}H]PCV for monitoring reporter gene expression of wild type and mutant herpes simplex virus type 1 thymidine kinase in cell culture. *Mol Imaging Biol.* 2005;7:296–303.
2. Min JJ, Iyer M, Gambhir SS. Comparison of [^{18}F]FHBG and [^{14}C]FIAU for imaging of HSV1-tk reporter gene expression: adenoviral infection vs stable transfection. *Eur J Nucl Med Mol Imaging.* 2003;30:1547–1560.
3. Sun H, Collins JM, Mangner TJ, Muzik O, Shields AF. Imaging the pharmacokinetics of [F-18]FAU in patients with tumors: PET studies. *Cancer Chemother Pharmacol.* 2005;57:1–6.
4. Bettegowda C, Foss CA, Cheong I, et al. Imaging bacterial infections with radiolabeled 1-(2′-deoxy-2′-fluoro-beta-D-arabinofuranosyl)-5-iodouracil. *Proc Natl Acad Sci U S A.* 2005;102:1145–1150.
5. Jacobs A, Voges J, Reszka R, et al. Positron-emission tomography of vector-mediated gene expression in gene therapy for gliomas. *Lancet.* 2001;358:727–729.
6. Jacobs A, Braunlich I, Graf R, et al. Quantitative kinetics of [^{124}I]FIAU in cat and man. *J Nucl Med.* 2001;42:467–475.
7. Mangner TJ, Klecker RW, Anderson L, Shields AF. Synthesis of 2′-deoxy-2′-[^{18}F]fluoro-beta-D-arabinofuranosyl nucleosides, [^{18}F]FAU, [^{18}F]FMAU, [^{18}F]FBAU and [^{18}F]FIAU, as potential PET agents for imaging cellular proliferation: synthesis of [^{18}F]labelled FAU, FMAU, FBAU, FIAU. *Nucl Med Biol.* 2003;30:215–224.
8. Nimmagadda S, Mangner TJ, Sun H, et al. Biodistribution and radiation dosimetry estimates of 1-(2′-deoxy-2′-^{18}F-fluoro-1-β-D-arabinofuranosyl)-5-bromouracil: PET imaging studies in dogs. *J Nucl Med.* 2005;46:1916–1922.
9. Stabin MG, Siegel JA. Physical models and dose factors for use in internal dose assessment. *Health Phys.* 2003;85:294–310.
10. Doubrovin M, Ponomarev V, Beresten T, et al. Imaging transcriptional regulation of p53-dependent genes with positron emission tomography in vivo. *Proc Natl Acad Sci U S A.* 2001;98:9300–9305.
11. Dubey P, Su H, Adonai N, et al. Quantitative imaging of the T cell antitumor response by positron-emission tomography. *Proc Natl Acad Sci U S A.* 2003;100: 1232–1237.
12. Koehne G, Doubrovin M, Doubrovina E, et al. Serial in vivo imaging of the targeted migration of human HSV-TK-transduced antigen-specific lymphocytes. *Nat Biotechnol.* 2003;21:405–413.
13. Shah K, Bureau E, Kim DE, et al. Glioma therapy and real-time imaging of neural precursor cell migration and tumor regression. *Ann Neurol.* 2005;57: 34–41.
14. Tamura M, Unno K, Yonezawa S, et al. In vivo trafficking of endothelial progenitor cells their possible involvement in the tumor neovascularization. *Life Sci.* 2004;75:575–584.
15. Tjuvajev JG, Avril N, Oku T, et al. Imaging herpes virus thymidine kinase gene transfer and expression by positron emission tomography. *Cancer Res.* 1998;58: 4333–4341.
16. Tjuvajev JG, Finn R, Watanabe K, et al. Noninvasive imaging of herpes virus thymidine kinase gene transfer and expression: a potential method for monitoring clinical gene therapy. *Cancer Res.* 1996;56:4087–4095.
17. Wang J, Eriksson S. Phosphorylation of the anti-hepatitis B nucleoside analog 1-(2′-deoxy-2′-fluoro-1-beta-D-arabinofuranosyl)-5-iodouracil (FIAU) by human cytosolic and mitochondrial thymidine kinase and implications for cytotoxicity. *Antimicrob Agents Chemother.* 1996;40:1555–1557.
18. Buursma AR, Rutgers V, Hospers GA, Mulder NH, Vaalburg W, de Vries EF. ^{18}F-FEAU as a radiotracer for herpes simplex virus thymidine kinase gene expression: in-vitro comparison with other PET tracers. *Nucl Med Commun.* 2006;27:25–30.
19. Klecker RW, Katki AG, Collins JM. Toxicity, metabolism, DNA incorporation with lack of repair, and lactate production for 1-(2′-fluoro-2′-deoxy-beta-D-arabinofuranosyl)-5-iodouracil in U-937 and MOLT-4 cells. *Mol Pharmacol.* 1994;46:1204–1209.
20. Richardson FC, Engelhardt JA, Bowsher RR. Fialuridine accumulates in DNA of dogs, monkeys, and rats following long-term oral administration. *Proc Natl Acad Sci U S A.* 1994;91:12003–12007.
21. Sun H, Collins JM, Mangner TJ, Muzik O, Shields AF. Imaging [^{18}F]FAU [1-(2′-deoxy-2′-fluoro-beta-D-arabinofuranosyl) uracil] in dogs. *Nucl Med Biol.* 2003; 30:25–30.
22. Vaidyanathan G, Zalutsky MR. Preparation of 5-[^{131}I]iodo- and 5-[^{211}At]astato-1-(2-deoxy-2-fluoro-beta-D-arabinofuranosyl) uracil by a halodestannylation reaction. *Nucl Med Biol.* 1998;25:487–496.
23. Fu D, Pomper MG, Foss CA, Ambinder R. Visualizing induction of lytic gamma herpesvirus infection. In: International Meeting of The Institute of Human Virology; Baltimore, MD: *Retrovirology.* 2005(suppl 1):S22.
24. Fu D, Lemas V, Foss C, Fox J, Pomper M, Ambinder RF. Enzymatically-targeted ^{131}I therapy for herpesvirus-associated malignancies. In: 2006 ASCO Annual Meeting Proceedings, part I: *J Clin Oncol.* 2006;P123S:3010.